Many-Body Quantum Dynamics of Polarization Squeezing in Optical Fibers

Joel F. Corney[*] and Peter D. Drummond

*ARC Centre of Excellence for Quantum-Atom Optics, The University of Queensland,
Brisbane, QLD 4072, Australia*

Joel Heersink, Vincent Josse, Gerd Leuchs, and Ulrik L. Andersen

*Institut für Optik, Information und Photonik, Max-Planck Forschungsgruppe, Universität Erlangen-Nürnberg,
Erlangen 91058, Germany*

We report new experiments that test quantum dynamical predictions of polarization squeezing for ultrashort photonic pulses in a birefringent fiber, including all relevant dissipative effects. This exponentially complex many-body problem is solved by means of a stochastic phase-space method. The squeezing is calculated and compared to experimental data, resulting in excellent quantitative agreement. From the simulations, we identify the physical limits to quantum noise reduction in optical fibers. The research represents a significant experimental test of first-principles time-domain quantum dynamics in a one-dimensional interacting Bose gas coupled to dissipative reservoirs.

The nonlinear optical response of standard communications fiber provides a straightforward and robust method [1] for squeezing the quantum noise always present in laser light to below the vacuum noise level. This feature allows us to design quantum dynamical experiments [2,3] operating in a very nonclassical regime where highly entangled states can be readily produced, even in many-body regimes involving 10^8 interacting particles. The squeezing is sensitive to photon-photon interactions, as well as to additional dissipative and thermal effects [4]. Such complications have affected all prior experiments and have so far prevented quantitative agreement between theory and experiment.

Here we report on quantitative comparisons of first-principles simulations with experimental measurements on the propagation of quantum states in optical fiber. The excellent agreement, over a wide range of initial conditions, is unprecedented for direct predictions from *ab initio* treatments of many-body quantum time evolution. The approach we use has potential applications in many other areas of science, especially to dynamical experiments with ultracold atoms and nanotechnology.

Photons in a nonlinear fiber are an implementation of the famous one-dimensional attractive Bose-gas model [5]. Fiber squeezing experiments thus provide a substantial opportunity to carry out an experimental test of the predictions of many-body quantum mechanics for dynamical time evolution. Such a test requires the same ingredients as did Galileo's famous tests of classical dynamics using an inclined plane [6]: one needs a known initial condition, a well-defined cause of dynamical evolution, and accurate measurements. All of these essential features are present in our experiments. The initial condition is a coherent [7] photonic state provided by a well-stabilized pulsed laser. The Kerr nonlinearity in silica fiber corresponds to a localized (delta-function) interaction between the photons [8]. Quantum-limited phase-sensitive measurements have been developed in optics that detect quantum fluctuations at well below the vacuum noise level [9,10].

Even though the simplest model of a 1D interacting Bose gas has exactly soluble energy eigenvalues, the many-body initial-value problem still remains intractably complex. Expanding the coherent initial state directly in terms of more than 10^{100} relevant eigenstates (more than the number of particles in the universe) is simply not practical. For such reasons, Feynman suggested [11] that the calculation of dynamical quantum time evolution would be impossible without special "quantum computing" hardware, which is not available at present. Even worse, there are additional complications occurring due to coupling to phonons in the silica fiber medium.

To deal with the exponential quantum complexity in this dissipative system, using existing computers, we employ quantum phase-space methods based on the work of Wigner [12] and Glauber [7]. With modifications to treat nonclassical fields [13], phase-space methods are able to calculate quantum correlations in a dynamical system without recourse to hydrodynamic approximations or linear response theory. They were successfully used for the original prediction of quantum squeezing in optical fibers, [14], which was qualitatively verified in several laboratories [1,15]. Recently, photon-number squeezing was simulated [16] and compared with experiment [17]. However, the cause of squeezing degradation was unclear [18]. By using an improved experimental configuration [3], and including all relevant dissipative effects in the simulations, we have been able to quantitatively test and verify the phase-space predictions.

Physically, the Kerr effect that generates the squeezing can be viewed as producing an intensity-dependent refrac-

tive index, which distorts an initially symmetric phase-space distribution into an ellipse. Because of energy conservation, however, the variance in the amplitude remains constant. Thus the squeezing cannot be detected directly in amplitude or intensity measurements.

Although laser homodyne measurements [10] can be used for these phase-sensitive measurements, they require a local oscillator, which is impractical for the high-intensity laser pulses used here. Instead, we employ an interferometric method known as polarization squeezing [3], wherein two multiphoton femtosecond pulses that are initially identical in amplitude propagate along the mutually orthogonal polarization axes x and y of a polarization-maintaining fiber. The two output pulses are then combined on a half-wave plate at an angle Φ. For the appropriate phase-space rotation angles $\theta = 4\Phi$, the squeezing or antisqueezing can be detected in the number difference. Because both pulses undergo similar evolution, most excess thermal noise is common to both modes and is thus cancelled. An exception here is any noise induced by birefringent, or depolarizing, effects. The experimental setup is illustrated in Fig. 1.

Because the experiment involves ultrashort pulses, we use photon-density operators for each polarization mode of the optical field: $\hat{\Psi}_x(t, z)$ and $\hat{\Psi}(t, z)$ that include a range of spectral components $\hat{a}(t, k)$:

$$\hat{\Psi}_\sigma(t, z) \equiv \frac{1}{\sqrt{2\pi}} \int dk \hat{a}_\sigma(t, k) e^{i(k-k_0)z + i\omega_0 t}, \quad (1)$$

where $\sigma = x, y$ labels the polarization, t is time, z is propagation distance, and k is the wave number. The wave number and frequency of the carrier wave are given
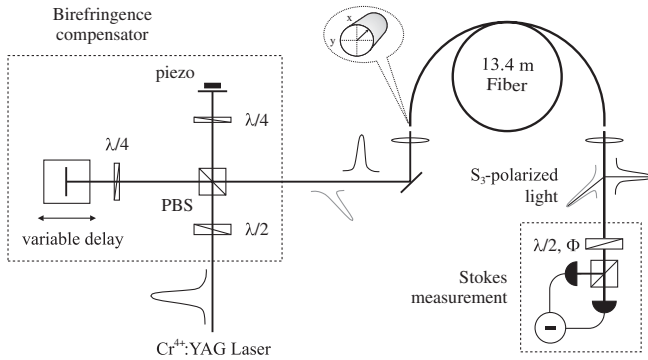

FIG. 1. Experimental detail for the efficient generation of polarization-squeezed states. Pairs of coherent, 130 fs FWHM sech-shaped laser pulses at 1.5 μm are coupled into a birefringent fiber. A prefiber variable delay ensures that the pulses overlap upon exiting the fiber. A relative phase shift of $\frac{\pi}{2}$ is maintained by means of a piezoelectric crystal in a feedback loop, resulting in circularly or S_3-polarized light. The squeezing measurement is performed by use of a half-wave plate, polarizing beam splitter and two balanced detectors. Although the squeezing is broadband, it is sampled at a frequency of 17.5 MHz to avoid technical noise.

by k_0 and ω_0. The commutation relations of the field operators are $[\hat{\Psi}_\sigma(t, z), \hat{\Psi}_{\sigma'}^\dagger(t, z')] = \delta(z - z')\delta_{\sigma\sigma'}$.

To describe the polarization squeezing, we define generalized Stokes operators:

$$\begin{aligned} \hat{S}_0 &\equiv \hat{N}_{xx}(L) + \hat{N}_{yy}(L), \quad \hat{S}_1 \equiv \hat{N}_{xx}(L) - \hat{N}_{yy}(L), \\ \hat{S}_2 &\equiv \hat{N}_{xy}(L) + \hat{N}_{yx}(L), \quad \hat{S}_3 \equiv i\hat{N}_{yx}(L) - i\hat{N}_{xy}(L), \end{aligned} \quad (2)$$

where L is the fiber length and $\hat{N}_{\sigma\sigma'}(z) = \int dt \hat{\Psi}_\sigma^\dagger(t, z)\hat{\Psi}_{\sigma'}(t, z)$. $\hat{S}_0$ corresponds to the combined intensity, $\hat{S}_1$ gives the number difference between the x and y modes, and $\hat{S}_2$ and $\hat{S}_3$ are operators sensitive to the relative phase difference. In the Stokes measurement after the fiber, we measure a given Stokes parameter orthogonal to the bright excitation in $\hat{S}_3$. This, the dark $\hat{S}_1$-$\hat{S}_2$ plane, is scanned by rotating a half-wave plate to measure $\hat{S}_\theta = \cos(\theta)\hat{S}_1 + \sin(\theta)\hat{S}_2$. Following from the Stokes operator commutation relations [19], the number difference is squeezed if the variance of $\hat{S}_\theta$ is below, for S_3-polarized light,

$$\Delta^2 \hat{S}_\theta < |\langle\hat{S}_3\rangle| = |\langle\hat{S}_0\rangle|. \quad (3)$$

To simulate the evolution of the photon density $\hat{\Psi}_\sigma(t, z)$, we employ a quantum model of a radiation field propagating along a fused silica fiber, including the $\chi^{(3)}$ nonlinear responses of the material and the nonresonant coupling to phonons [4,20]. The phonons act as a reservoir with finite-time correlations (non-Markovian) that generates additional, delayed nonlinearity, as well as spontaneous and thermal noise. Classical, low-frequency phase noise can be neglected, because it is common to both polarization modes, unless there is a depolarizing component. The phonon spectrum is based on the experimentally determined Raman gain for pure fused silica $\alpha^R(\omega)$ [21]. Because of the fiber birefringence, the two polarization components do not temporally overlap for most of the fiber length, so we neglect the cross-polarization component of the Raman gain.

To simplify the theoretical description, we use a propagative frame with rescaled time $\tau \equiv (t - z/v)$, rescaled propagation distance $\zeta \equiv z/z_0$, and dimensionless photon-flux field $\hat{\phi}_\sigma \equiv \hat{\Psi}_\sigma\sqrt{vt_0/\bar{n}}$. Here t_0 is the pulse duration, $z_0 \equiv t_0^2/|k''|$ is the dispersion length, and $2\bar{n}$ is the photon number in a fundamental $\mathrm{sech}(\tau)$ soliton pulse. Other parameters are pulse velocity v, and dispersion parameter k''.

From the multimode Hamiltonian for the full system [4], we obtain Heisenberg equations of motion for the quantum fields. The phonon equations are integrated to derive quantum Langevin equations for the photon-flux field

$$\frac{\partial}{\partial \zeta}\hat{\phi}_\sigma(\tau,\zeta) = \frac{i}{2}\frac{\partial^2}{\partial\tau^2}\hat{\phi}_\sigma(\tau,\zeta) + i\hat{\Gamma}_\sigma(\tau,\zeta)\hat{\phi}_\sigma(\tau,\zeta) + i\int_{-\infty}^{\infty} d\tau' h(\tau-\tau')\hat{\phi}_\sigma^\dagger(\tau',\zeta)\hat{\phi}_\sigma(\tau',\zeta)\hat{\phi}_\sigma(\tau,\zeta),\tag{4}$$

where the nonlinear response function $h(\tau)$ includes both the instantaneous electronic response and the Raman response determined by the gain function $\alpha^R(\omega)$ [4,20,21]. The correlations of the reservoir fields are

$$\langle\hat{\Gamma}_\sigma^\dagger(\omega',\zeta')\hat{\Gamma}_{\sigma'}(\omega,\zeta)\rangle = \frac{\alpha^R(|\omega|)}{\bar{n}}[n_{\text{th}}(|\omega|)+\Theta(-\omega)]$$
$$\times\,\delta(\zeta-\zeta')\delta(\omega-\omega')\delta_{\sigma\sigma'},\tag{5}$$

where n_{th} is the temperature-dependent Bose distribution of phonon occupations. The Stokes ($\omega<0$) and anti-Stokes ($\omega>0$) contributions to the Raman noise are included by means of the step function Θ. These equations can easily be modified to include coupling to gain and absorption reservoirs, but this is unnecessary for the short distances in these experiments.

The exact quantum dynamics can be simulated using the positive-P ($+P$) phase-space representation [14]. However, for large photon number $\bar{n}$ and short propagation distance L, it is known that the $+P$ method gives squeezing predictions in agreement with a truncated Wigner phase-space method [22], which allows faster calculations. We have chosen the latter method to reduce computational overheads. This method maps a field operator to a stochastic field: $\hat{\phi}_\sigma(\zeta,\tau)\rightarrow\phi_\sigma(\zeta,\tau)$, with stochastic averages corresponding to symmetrically ordered correlations of the quantum system. Because of the symmetric-ordering correspondence, quantum effects enter via vacuum noise. The Kerr effect merely amplifies or diminishes this noise in a phase-sensitive manner, which makes the Wigner approach ideally suited for squeezing calculations.

Using the Wigner mapping, we obtain a Raman-modified stochastic nonlinear Schrödinger equation for the photon flux that is of exactly the same form as Eq. (4) [4,20]. The correlations of the Raman noise fields Γ_σ are also of the same form as their operator equivalent Eq. (5), except that the step function is replaced by a constant $1/2$. Because of the symmetrically ordered mapping, the Stokes and anti-Stokes contributions to the Wigner Raman noise are identical. The initial condition of the stochastic field is the mean coherent level plus fluctuations that correspond to vacuum noise:
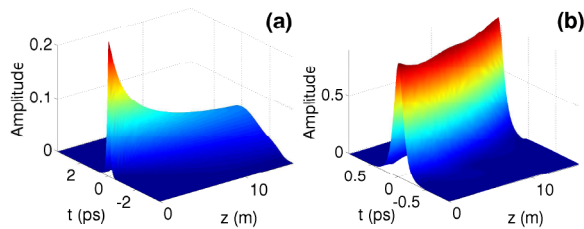
$$\langle\Delta\phi_\sigma(\tau,0)\Delta\phi_{\sigma'}^*(\tau',0)\rangle = \frac{1}{2\bar{n}}\delta(\tau-\tau')\delta_{\sigma\sigma'}.\tag{6}$$

Simulations [23] of the pulse propagation reveal the importance of including the system's multimode nature, which affects small-amplitude and intense pulses in different ways. As Fig. 2 shows, the evolution of the amplitude profile of a weak pulse is dominated by dispersion. In contrast, an intense pulse reshapes into a soliton, whose subsequent evolution reveals the effect of the Raman self-frequency shift. The range of input pulse energies in the experiment includes both of these extremes.

Figure 3 gives the phase-space rotation angle θ at which squeezing is observed at different input energies. The simulations and experiments agree very well for the intense pulses, but there is a divergence for weak pulses. Now classical phase noise has a relatively strong effect on the weaker pulses, because the antisqueezing produced by the Kerr effect is then smaller and at a greater angle to the phase quadrature. We therefore include the effect of excess phase noise by a nonlinear least-squares procedure. A new relative noise variance is calculated from

$$\Delta^2\hat{S}_\theta/\langle\hat{S}_3\rangle = \rho_p\sin^2(\theta_N) + \rho_s\cos^2(\theta_N-\theta_K)$$
$$+\rho_a\sin^2(\theta_N-\theta_K),\tag{7}$$

where $\theta_K(E)$ are the angles for Kerr squeezing with input energy E, and where $\rho_s(E)$, $\rho_a(E)$, and $\rho_p(E)$ are the relative variances of the Kerr squeezing, Kerr antisqueezing, and phase noise. The Kerr variances and angles $\theta_K(E)$ are taken from the simulation data, and the phase noise is assumed to depend linearly on pulse energy [24]. The coefficient of the phase noise is determined by a nonlinear least-squares fit of the angles $\theta_N(E)$ that minimize the new variance to the measured squeezing angles. The result gives an excellent fit to the experimental data, even though there is only one parameter for each fiber length. This parameter was larger for the longer fiber length, indicating
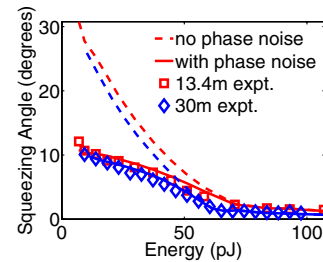

FIG. 2 (color online). Propagation of (a) $E=4.8$ pJ and (b) $E=53.5$ pJ pulses, with initial width $t_0=74$ fs.

FIG. 3 (color online). Phase-space rotation angle θ versus total input energy E. Squares and diamonds give the experimental results for the $L_1=13.4$ m and $L_2=30$ m fibers, respectively. Continuous (dashed) lines give the simulation results with (without) excess phase noise. Other parameters are $t_0=74$ fs, $z_0=0.52$ m, $\bar{n}=2\times10^8$, and $\lambda_0=1.51$ μm.
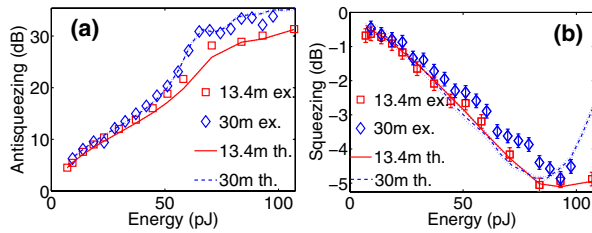
FIG. 4 (color online).   Raw antisqueezing (a) and squeezing (b) for $L_1 = 13.4$ m (squares) and $L_2 = 30$ m (diamonds) fibers. Error bars on the squeezing data indicate the uncertainty in the noise measurement; for the antisqueezing, the error bars were too small to be plotted distinctly. Solid and dashed lines show the simulation results with additional phase noise for L_1 and L_2, respectively. Dotted lines indicate the sampling error in the simulation results.

that phase noise is largely a fiber-induced effect, such as depolarizing guided acoustic wave Brillouin scattering (GAWBS). However, there also seems to be a smaller birefringent noise source outside the fiber.

Antisqueezing and squeezing results are shown in Fig. 4, for 13.4 and 30 m of fiber, with the excess phase noise included. The theoretical results for both squeezing and antisqueezing closely match the experimental data, after estimated linear losses of 24% are taken into account. That the theoretical antisqueezing results match the experiment indicates that the fit obtained from the rotation angle accounts for all the excess classical noise. A deterioration of the squeezing is seen at higher intensity due to Raman effects, especially for longer fiber lengths.

As an indication of the accuracy of the simulations, we predicted from comparisons of the rotation angle and the antisqueezing curves in theory and in experiment that the 30 m fiber should have a 5% larger core diameter than the shorter fiber. This was verified by fiber measurements. There is a residual discrepancy in the highly sensitive squeezing measurements for the 30 m case at large pulse energies. This could be due to effects such as cross-polarization Raman scattering, higher-order dispersion, or initial pulse-shape distortion.

In conclusion, the efficiency of the squeezing experiments described here means that a comprehensive theoretical model must be formulated and solved to quantitatively account for all observations. Solving the model requires a first-principles simulation of quantum time evolution in a many-body system coupled to a non-Markovian reservoir. We have achieved this by means of a Wigner phase-space representation, thus obtaining excellent agreement between simulation and experiment over a wide range of energies and fiber lengths. The simulations reveal that Raman effects limit squeezing at high intensity and for longer fibers and that depolarizing phase noise (i.e., GAWBS) limits squeezing at low intensity.

*Electronic address: corney@physics.uq.edu.au
[1] P. D. Drummond, R. M. Shelby, S. R. Friberg, and Y. Yamamoto, Nature (London) **365**, 307 (1993).
[2] A. Sizmann and G. Leuchs, Prog. Opt. **39**, 373 (1999).
[3] J. Heersink, V. Josse, G. Leuchs, and U. L. Andersen, Opt. Lett. **30**, 1192 (2005).
[4] P. D. Drummond and J. F. Corney, J. Opt. Soc. Am. B **18**, 139 (2001).
[5] J. B. McGuire, J. Math. Phys. (N.Y.) **5**, 622 (1964).
[6] G. Galilei, *Discorsi e Dimostrazioni Matematiche, Intorno á due Nuoue Scienzes* (Appresso gli Elsevirii, Leiden, 1638) [translation S. Drake, (University of Wisconsin, Madison, 1974)].
[7] R. J. Glauber, Phys. Rev. **130**, 2529 (1963).
[8] B. Yurke and M. J. Potasek, J. Opt. Soc. Am. B **6**, 1227 (1989).
[9] D. F. Walls, Nature (London) **306**, 141 (1983); R. Loudon and P. L. Knight, J. Mod. Opt. **34**, 709 (1987).
[10] P. D. Drummond and Z. Ficek, *Quantum Squeezing* (Springer-Verlag, Berlin, Heidelberg, New York, 2004).
[11] R. P. Feynman, Int. J. Theor. Phys. **21**, 467 (1982).
[12] E. P. Wigner, Phys. Rev. **40**, 749 (1932).
[13] P. D. Drummond and C. W. Gardiner, J. Phys. A **13**, 2353 (1980).
[14] S. J. Carter, P. D. Drummond, M. D. Reid, and R. M. Shelby, Phys. Rev. Lett. **58**, 1841 (1987); P. D. Drummond and S. J. Carter, J. Opt. Soc. Am. B **4**, 1565 (1987).
[15] M. Rosenbluh and R. M. Shelby, Phys. Rev. Lett. **66**, 153 (1991).
[16] M. J. Werner, *ibid.* **81**, 4132 (1998).
[17] S. Schmitt, J. Ficker, M. Wolff, F. König, A. Sizmann, and G. Leuchs, Phys. Rev. Lett. **81**, 2446 (1998).
[18] M. Fiorentino, J. E. Sharping, P. Kumar, D. Levandovsky, and M. Vasilyev, Phys. Rev. A **64**, 031801 (2001).
[19] M. Kitagawa and M. Ueda, Phys. Rev. A **47**, 5138 (1993); N. Korolkova, G. Leuchs, R. Loudon, T. C. Ralph, and Ch. Silberhorn, *ibid.* **65**, 052306 (2002).
[20] S. J. Carter and P. D. Drummond, Phys. Rev. Lett. **67**, 3757 (1991).
[21] R. H. Stolen, C. Lee, and R. K. Jain, J. Opt. Soc. Am. B **1**, 652 (1984).
[22] P. D. Drummond and A. D. Hardman, Europhys. Lett. **21**, 279 (1993).
[23] The simulations were performed by means of the XMDS code-generating package (http://www.xmds.org). The phase-space equations were discretized on a regular grid ($\Delta\tau \simeq 0.2$, $\Delta\zeta \simeq 0.03$) and solved by a split-step Fourier method, with an iterative semi-implicit algorithm for the nonlinear and stochastic terms. The non-Markovian reservoirs were included by explicitly integrating a set of phonon variables at each point in the propagation grid. Physical quantities were calculated by stochastic averages over 10 000 runs.
[24] R. M. Shelby, P. D. Drummond, and S. J. Carter, Phys. Rev. A **42**, 2966 (1990).